Dynamic relocalization of the cytosolic type III secretion system components prevents premature protein secretion at low external pH

Stephan Wimmi[1], Alexander Balinovic[2], Hannah Jeckel[2,3], Lisa Selinger[1], Dimitrios Lampaki[1], Emma Eisemann[1*], Ina Meuskens[4], Dirk Linke[4], Knut Drescher[2,3], Ulrike Endesfelder[2] & Andreas Diepold[1]*

1: Max Planck Institute for Terrestrial Microbiology, Department of Ecophysiology, Karl-von-Frisch-Str. 10, 35043 Marburg, Germany

2: Max Planck Institute for Terrestrial Microbiology, Karl-von-Frisch-Str. 10, 35043 Marburg, Germany

3: Department of Physics, Philipps-Universität Marburg, Karl-von-Frisch-Str. 16, 35043 Marburg, Germany

4: University of Oslo, Department of Biosciences, Blindernveien 31, 0371 Oslo, Norway

* current addresses:

Dimitrios Lampaki, Max-Planck-Institut für Immunbiologie und Epigenetik, Stübeweg 51, 79160 Freiburg, Germany;
Emma Eisemann, James Madison University, 800 South Main St, Harrisonburg, VA 22807, USA

Correspondence: Andreas Diepold, andreas.diepold@mpi-marburg.mpg.de, +49-6421-178302

Running title: Dynamic pH adaptation of the T3SS

Abstract

Many bacterial pathogens use a type III secretion system (T3SS) to manipulate host cells. Protein secretion by the T3SS injectisome is activated upon contact to any host cell, and it has been unclear how premature secretion is prevented during infection. We found that in gastrointestinal pathogens, cytosolic injectisome components are temporarily released from the proximal interface of the injectisome at low external pH, preventing protein secretion in acidic environments, such as the stomach. In *Yersinia enterocolitica*, low external pH is detected in the periplasm and leads to a partial dissociation of the inner membrane injectisome component SctD, which in turn causes the dissociation of the cytosolic T3SS components. This effect is reversed upon restoration of neutral pH, allowing a fast activation of the T3SS at the native target regions within the host. These findings indicate that the cytosolic components form an adaptive regulatory interface, which regulates T3SS activity in response to environmental conditions.

Introduction

In order to proliferate in contact to eukaryotic host cells, both symbiotic and pathogenic bacteria have developed methods to influence host cell behavior. The type III secretion system (T3SS) injectisome is a molecular machinery used by various pathogenic bacterial genera including *Salmonella, Shigella,* pathogenic *Escherichia*, *Pseudomonas* and *Yersinia* to deliver molecular toxins – effector proteins – directly into the eukaryotic host cells. While the effectors differ among the different bacterial species (Büttner, 2012), and can have different functions in modulating the cytoskeleton, invading and escaping host cells or endosomes, or inducing host cell death (Hueck, 1998; Coburn *et al*, 2007), the structural proteins of the injectisome are highly conserved (Deng *et al*, 2017; Wagner *et al*, 2018). An extracellular needle is formed by helical polymerization of a T3SS-exported protein, and ends in a pentameric tip structure. At the proximal end, the needle is anchored by two multimeric membrane rings that span the outer and inner membrane. Additionally, the inner membrane (IM) ring encloses the export apparatus. At the cytosolic interface of the injectisomes, four soluble T3SS components (SctK/Q/L/N)[a] interact to form six pod structures (Hu *et al*, 2015, 2017) (Fig. 1A).

The soluble T3SS components SctK, SctQ, SctL and SctN interact in a linear fashion (Jackson & Plano, 2000), and the presence of all four proteins is needed for their assembly at the injectisome, and subsequently for effector secretion (Diepold *et al*, 2010, 2017). SctK/Q/L form a high molecular weight complex that has been shown to bind chaperones and effectors (Lara-Tejero *et al*, 2011). Since the cytosolic components do not co-purify with the rest of the needle, their structural arrangement has only been revealed by recent *in situ* cryo-electron tomography (Hu *et al*, 2015; Nans *et al*, 2015; Makino *et al*, 2016; Hu *et al*, 2017), which showed the formation of six pod structures at the cytosolic interface of the injectisome. The connection between these pod structures and the membrane rings is established by the cytosolic component SctK, which binds to SctD. In the presence of SctK, the cytosolic domains of SctD ($SctD_C$) rearrange and in the case of the *Salmonella* SPI-1 T3SS form six discrete patches of four $SctD_C$ each that interact with one SctK protein, which in turn connects to SctQ, SctL, and SctN (Hu *et al*, 2017; Tachiyama *et al*, 2019).

In addition to forming the injectisome-bound pod structures, the cytosolic components exist in a freely diffusing cytosolic state, with proteins exchanging between the two states (Diepold *et al*, 2015). In the cytosol, SctK/Q/L/N form a dynamic adaptive network, with a variety of complexes of different stoichiometries that change their composition in response to different external conditions (Diepold *et al*, 2017; Bernal *et al*, 2019). Strikingly, protein interactions and exchange rates amongst the cytosolic

[a] In this manuscript, T3SS refers to the virulence-associated T3SS. The common „Sct“ nomenclature (Hueck, 1998) is used for T3SS components, see (Diepold & Wagner, 2014) for species-specific names.

components correlate with the activity of the injectisome (Diepold *et al*, 2017; Rocha *et al*, 2018; Diepold *et al*, 2015). However, the precise role of the cytosolic components in the secretion process remains unclear to this date.

Yersinia enterocolitica is an extracellular gastrointestinal pathogen that employs its T3SS to downregulate immune responses and prevent inflammation after the penetration of the intestinal epithelium. For initial attachment to the epithelium, the bacteria employ a number of adhesins, with *Yersinia* adhesin A (YadA) as the key factor for establishing an infection (Meuskens *et al*, 2019). YadA interacts with a variety of extracellular matrix molecules, including collagen and fibronectin (Mühlenkamp *et al*, 2015). YadA length is tightly linked to the length of the injection needle of the T3SS, and establishes close contact to the host cells enabling injection (Mota *et al*, 2005). *Y. enterocolitica* is usually taken up with contaminated food or water. The shift from environmental to host temperature (37°C) induces expression and assembly of the injectisomes as well as YadA (Tertti *et al*, 1992; Cornelis, 2006). The bacteria then have to pass the acidic environment of the stomach. During that time, the injectisome can already be present and ready for secretion of translocators (which form a pore in the host membrane and its connection to the needle, Fig. 1A) and effectors. Since the T3SS readily translocates cargo into any host cell type it adheres to, including immune cells, epithelial cells and even red blood cells (Clerc *et al*, 1986; Håkansson *et al*, 1996), a distinct mechanism is needed to prevent premature activation of the T3SS during the passage of the stomach, which would result in a loss of valuable resources, or even elicit immune responses.

We hypothesized that the acidic environment in the stomach (external pH of 1.5 – 4.5 (Evans *et al*, 1988; McClements & Li, 2010), Fig. 1B) may be detected by bacteria to inhibit effector secretion under these conditions. Here, we investigated this hypothesis with a combination of fluorescence microscopy, single particle tracking, and functional assays. Our findings show that although parts of the T3SS, including the extracellular needle, are stable at low pH, a set of cytosolic T3SS components temporarily unbind from the injectisome at low external pH. The reversible dissociation corresponds to a temporary suppression of effector secretion by the T3SS. This mechanism prevents premature activation of the T3SS, while ensuring a quick reactivation of the T3SS, once a pH-neutral environment is reached. Our data provide a striking example for how bacteria apply protein dynamics to adapt the function of a large macromolecular machine essential for virulence to external conditions.

77 **Results**

78 Resistance of *Y. enterocolitica* and its T3SS needles to low external pH

79 To investigate to which degree *Y. enterocolitica* can withstand a drop in external pH, cultures of
80 *Y. enterocolitica* IML421asd (a strain lacking the six main virulence effectors YopH,O,P,E,M,T)
81 (Kudryashev *et al*, 2013) in exponential growth phase were exposed to different pH for 15 minutes at
82 28°C. A subsequent dilution series on neutral pH agar showed nearly complete survival down to pH 4
83 (Fig. 1C). Likewise, bacterial cultures remained at a constant optical density at pH 4 at 37°C for at least
84 90 min, and recovered their growth upon restoration of neutral pH (Suppl. Fig. 1). Together, these
85 results show that *Y. enterocolitica* tolerates temporary incubation down to pH 3, with no or very little
86 fitness decrease at pH 4 and above.

87 *Y. enterocolitica* adheres to host cells and other surfaces by adhesins, most importantly the trimeric
88 adhesin YadA and invasin (Keller *et al*, 2015; Mühlenkamp *et al*, 2015; Leo *et al*, 2015). We thus tested
89 whether low pH prevents the binding of YadA to collagen and more generally, of *Y. enterocolitica* cells
90 to surfaces. Binding could be established at low pH in both cases (Fig. 1D, Suppl. Videos 1-2), albeit at
91 a reduced level (about 50% binding at pH 4). These results suggest that to avoid protein translocation
92 into non-host cells, secretion itself might be prevented at low pH.

93 To test under which conditions *Y. enterocolitica* secretes T3SS substrates, we performed an *in vitro*
94 secretion assay where *Y. enterocolitica* cells primed for secretion were subjected to secreting media in
95 the range from pH 8 to pH 4. Indeed, we observed that secretion did not occur at low pH (Fig. 1E, Suppl.
96 Fig. 2A). Lack of secretion is not due to lower protein synthesis at pH 4 (Suppl. Fig. 2B), suggesting a
97 specific mechanism to suppress secretion at low external pH.

98 But how does *Y. enterocolitica* prevent secretion at low pH? To determine if the absence of secretion
99 is due to a complete disassembly of injectisomes at that pH, we visualized the needles at different
100 pH values and over time by labeling an introduced cysteine residue with a maleimide-linked dye (Milne-
101 Davies *et al*, 2019). The needles were stable at pH 4 over continued time periods (Fig. 1F,
102 Suppl. Fig. 3).

103 Taken together, *Y. enterocolitica* as well as its injectisome needles can withstand low external pH
104 conditions, but still translocators and effectors are not secreted.

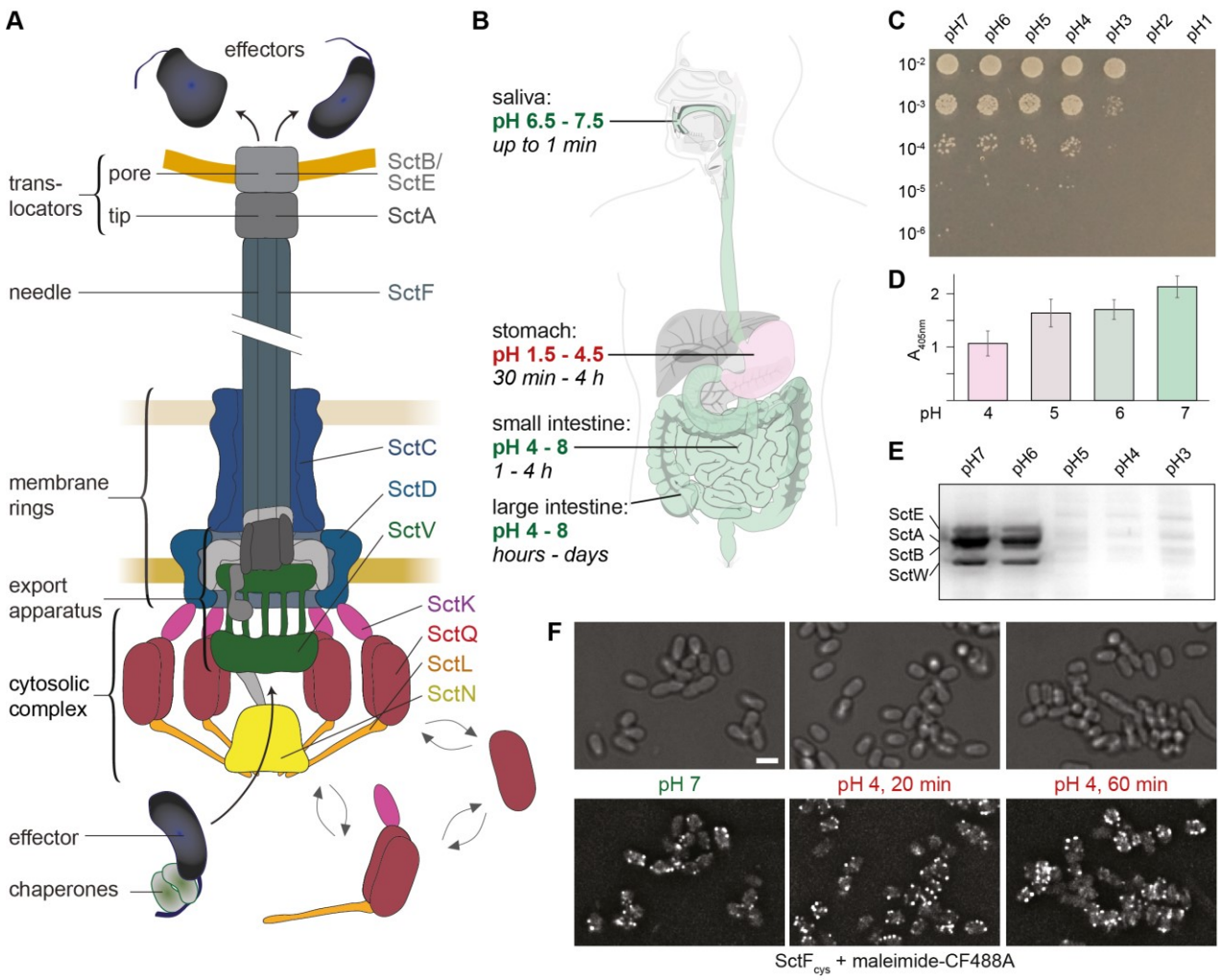

Fig. 1 – The *Yersinia enterocolitica* T3SS and its function and stability at low pH

(**A**) Schematic representation of the active T3SS injectisome (modified from (Diepold & Wagner, 2014)). Left side, description of main substructures; right side, names of T3SS components studied in this manuscript. Double arrows indicate the exchange of the cytosolic subunits or subcomplexes between the cytosolic and the injectisome-bound state. (**B**) pH ranges and typical retention times at different parts of the gastrointestinal system (Evans *et al*, 1988; McClements & Li, 2010). Digestive tract image based on the public domain template https://commons.wikimedia.org/wiki/File:Digestive_system_diagram_de.svg. (**C**) Dilution drop test of *Y. enterocolitica* cultures incubated at the indicated pH for 15 minutes. (**D**) Binding of the *Y. enterocolitica* adhesin YadA to collagen at the indicated pH values. Absorption at 405 nm resulting from Ni^{2+}-HRP binding to YadA-His_6 incubated with plate-absorbed calf collagen type I. n = 3, error bars denote standard deviation. (**E**) *In vitro* secretion assay showing the export of native T3SS substrates (indicated on left side) in strain IML421 at the indicated external pH values. Black and white scan of a coomassie-stained SDS-PAGE gel; supernatant of $3*10^8$ bacteria per lane. Secretion assay of strain containing effectors, see Suppl. Fig. 2A. (**F**) Staining of T3SS needles at the different indicated external pH values; time indicates the duration of pH 4 treatment. A strain expressing the mutated needle subunit $SctF_{cys}$ was covalently labeled with maleimide-CF488A. Scale bar, 2 µm.

123 Association of the dynamic cytosolic T3SS components to the injectisome is temporarily suppressed at
124 low external pH

125 We have recently found that the cytosolic T3SS components (SctK/Q/L/N) form a dynamic network,
126 where protein exchange is connected to the function of the injectisome (Fig. 1A) (Diepold *et al*, 2015,
127 2017). Hence, we wondered whether these dynamic components could be involved in the inhibition of
128 secretion at low pH. To investigate this question, we performed flow-cell-based total internal reflection
129 fluorescence (TIRF) microscopy with functional N-terminal fluorescent protein fusions of the cytosolic
130 components, expressed at native levels[b]: EGFP-SctK, EGFP-SctQ, EGFP-SctL and EGFP-SctN (Fig. 1A)
131 (Diepold *et al*, 2010, 2017). At neutral or near-neutral pH, the cytosolic components localized in foci at
132 the bacterial membrane, which represent their injectisome-bound state (Diepold *et al*, 2010). However,
133 at an external pH of 4, all cytosolic components lost this punctuate localization, and the proteins
134 relocated to the cytosol (Fig. 2 ABC). The relocation remained stable over time at low external pH
135 (Suppl. Fig. 4). Strikingly, this phenomenon was reversible: Upon exposure to neutral external pH, the
136 foci recovered within a few minutes (Fig. 2ABC). This effect was observed both under secreting and
137 non-secreting conditions (Suppl. Fig. 5A), and was independent of the fluorophore or visualization tag
138 that was used (Suppl. Fig. 5B). Dissociation and re-association of the cytosolic T3SS components in
139 response to the external pH was reversible for several cycles (Suppl. Video 3). This reversible response
140 to low pH was also observed both under secreting and non-secreting conditions (presence of 5 mM
141 $CaCl_2$ and EGTA, respectively) (Suppl. Fig. 6).

142 To determine the kinetics of association and dissociation of SctQ, we monitored EGFP-SctQ foci in a
143 microscopy flow cell after a pH drop from 7 to 4 and *vice versa*. Foci gradually disappeared within two
144 minutes under secreting condition (Fig. 2D, Suppl. Fig. 7, Suppl. Video 4). Upon restoration of neutral
145 external pH, the first distinct foci were visible after 50 seconds, and further increased in abundance
146 and brightness over time (Suppl. Fig. 8, Suppl. Video 5).

147 To test whether the recovery of foci was due to the synthesis of new proteins or if the previously bound
148 proteins rebind to the injectisomes, we covalently labeled the pool of Halo-tagged SctL with the Janelia
149 Fluor JF-646 Halo ligand dye (Grimm *et al*, 2017) prior to the incubation at pH 4 to ensure that only the
150 protein pool present at the time of labelling was fluorescent. Similar to the previous experiments, we
151 observed a reversible loss of fluorescent foci at the membrane and an increase in cytosolic signal at pH
152 4 and rebinding of the fluorescent proteins upon changing pH to 7 (Fig. 2C). Also, an overlay of the
153 micrograph at pH 7 before and after the incubation at pH 4 further indicated that most foci reform at

[b] All *Y. enterocolitica* fusion proteins used in this study are expressed from the native genetic environment; the genes replace the wild-type genes by allelic exchange (Kaniga *et al*, 1991).

154 the same position as they previously appeared (Fig. 2E), and colocalize with the T3SS needles (Suppl.
155 Fig. 9).

156 Taken together, our data indicate that the cytosolic components reversibly dissociate from the
157 injectisome at low external pH. Upon exposure to neutral pH, proteins from the same pool rebind at
158 the cytosolic interface of the injectisome, forming the potential basis for a regulatory mechanism for
159 the prevention of secretion at low pH.

160

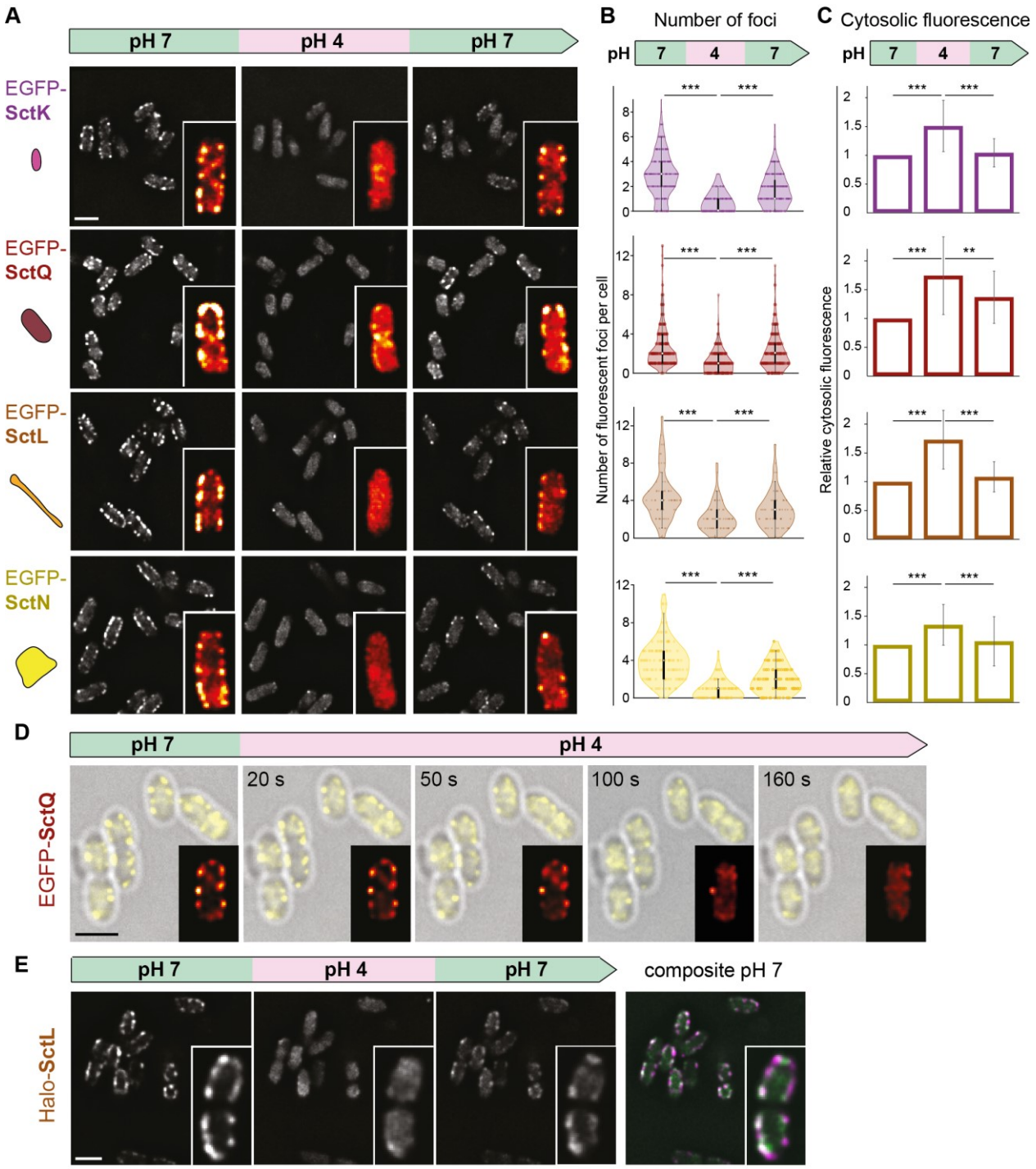

Fig. 2 – The cytosolic T3SS components temporarily dissociate from the injectisome at low external pH

(**A**) Fluorescent micrographs of the indicated proteins in live *Y. enterocolitica*, consecutively subjected to different external pH in a flow cell. Images were taken under secreting conditions, 10 minutes after bacteria were subjected to the indicated pH. Insets, enlarged single bacteria, visualized with the ImageJ red-hot color scale. (**B**) Quantification of foci per bacterium for the strains and conditions shown in panel (A). *n* = 324, 320, 220, 117 foci (from top to bottom) from 2-3 fields of view from a representative experiment. (**C**) Quantification of mean cytosolic fluorescence for the strains and conditions shown in panel (A). *n* = 50 cells from 2 independent experiments per strain. For (B) and (C), error bars denote standard deviation; */**/***, p<0.05/0.01/0.001 in homoscedastic two-tailed t-tests. The values at pH 7 before and after incubation at pH 4 differ statistically

171 significantly for (B) (***), but not for (C) (p>0.05), except for SctQ (***) and SctL (*). (**D**) Kinetics of EGFP-SctQ
172 dissociation after pH shift from 7 to 4. Overlay of phase contrast (grey) and fluorescence images (yellow); insets,
173 enlarged single bacterium, visualized with the ImageJ red-hot color scale. (**E**) Fluorescence micrographs of Halo-
174 SctL, labeled with JF-646 prior to the first image, during consecutive incubation at different external pH as in (A).
175 Right, overlay of fluorescence distribution at pH prior to and after pH 4 incubation (magenta and green,
176 respectively). Scale bars, 2 µm

177

178 Molecular mechanism of extracellular pH sensing

179 What is the molecular basis for the dissociation of the cytosolic T3SS components at low external pH?
180 To find out whether the pH is sensed intracellularly, we first tested the impact of the changed external
181 pH on the cytosolic pH, using a ratiometric pHluorin GFP variant (pHluorin$_{M153R}$ (Miesenböck *et al*, 1998;
182 Morimoto *et al*, 2011)) as a pH sensor. Upon changing the external pH from 7 to 4, the cytosolic pH
183 dropped to a mildly acidic value (pH 6.3-6.4). This cytosolic pH was retained for at least 30 minutes at
184 external pH 4, but quickly recovered upon re-establishment of neutral external pH (Fig. 3A).

185 To test if this mild drop in cytosolic pH directly causes the dissociation of the cytosolic complex, we
186 treated bacteria with the proton ionophore 2,4-dinitrophenol, which attunes the cytosolic pH to the
187 external pH (Hong *et al*, 1979; Dechant *et al*, 2010; Petrovska *et al*, 2014) (Suppl. Fig. 10), and visualized
188 the localization of EGFP-SctQ at different pH values. EGFP-SctQ remained localized in foci representing
189 assembled cytosolic complexes at pH 6.3 and below (Fig. 3B), indicating that the observed disassembly
190 of the cytosolic complex is not caused by acidification of the cytosol.

191

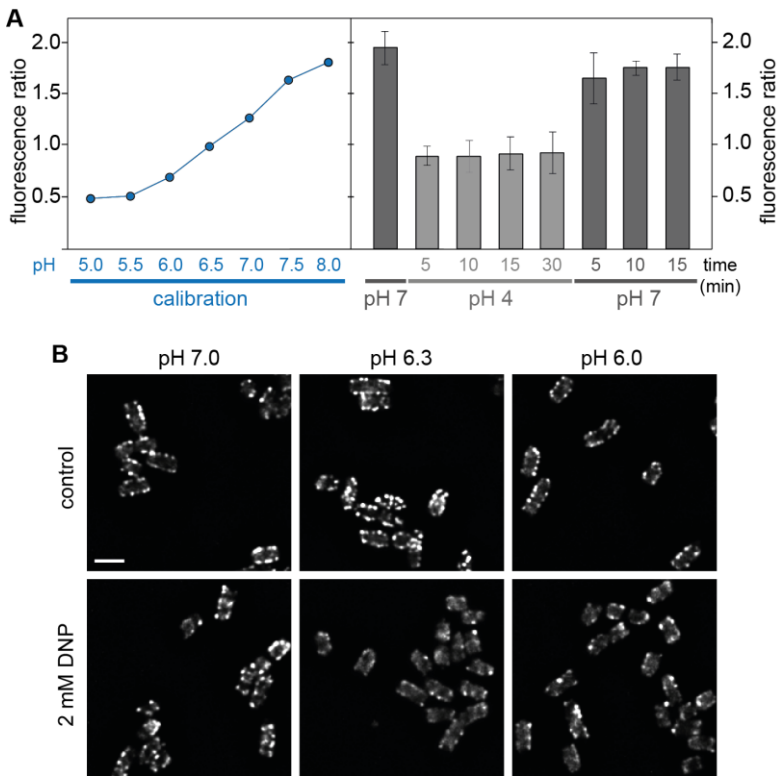

Fig. 3 – Low external pH leads to a small drop in cytosolic pH, which does not induce the dissociation of cytosolic T3SS components

(**A**) Left, calibration of (Ex_{390nm} / Ex_{475nm}) fluorescence ratio of purified $pHluorin_{M153R}$ for the indicated pH values. Technical triplicate, error bars too small to display. Right, determination of cytosolic pH upon changing the external pH from 7 (first column) to 4 (columns 2-5) and back (columns 6-8). Fluorescence ratio (Ex_{390nm} / Ex_{475nm}) of bacteria expressing cytosolic $pHluorin_{M153R}$. n = 4, error bars denote standard deviation. (**B**) Fluorescence distribution of EGFP-SctQ in live *Y. enterocolitica* at indicated external pH in absence (top) or presence (bottom) of the ionophore 2,4-dinitrophenol (DNP). At pH 4.0, no foci are present. Scale bar, 2 µm.

Based on above results, we searched for a periplasmic pH sensor. An obvious candidate is SctD, a bitopic IM protein connecting the outer membrane (OM) ring to the cytosolic components (Fig. 1A) (Ross & Plano, 2011; Hu *et al*, 2017). Earlier studies showed that lack of SctD, or its inability to bind to SctC, leads to a similar cytosolic location of SctK/L/N/Q as observed at an external pH of 4 (Fig. 2A) (Diepold *et al*, 2010, 2017), and that the cytosolic domains of SctD connect to SctK via specific interactions (with four SctD binding to one SctK in *Salmonella* SPI-1) (Hu *et al*, 2017; Tachiyama *et al*, 2019). This suggests that structural rearrangements of SctD could easily lead to dissociation of SctK and, subsequently, all other cytosolic components.

When we tested the behavior of SctD at low external pH, we found that at pH 4, EGFP-SctD foci in the membrane became less intense than at pH 7, with a concomitant increase in fluorescence throughout the membrane. In contrast to the cytosolic components however, the SctD foci did not completely disappear (Fig. 4A). Importantly, like the cytosolic components, SctD recovered its localization in foci at neutral external pH (Fig. 4A). To study this unique phenotype in more detail, we performed single-molecule tracking of PAmCherry-SctD proteins in photoactivated localization microscopy (PALM). These experiments revealed that at an external pH of 7, more than 90% of the SctD molecules in the IM were static; by contrast, at an external pH of 4, more than 40% of the SctD molecules became mobile

229 within the membrane (Fig. 4B, Suppl. Fig. 11), indicating a dissociation from the core injectisome
230 structure at low external pH. Indeed, the large T3SS export apparatus component SctV-EGFP retained
231 its localization within foci at pH 4; however, these foci (probably representing the SctV nonamers) were
232 mobile within the membrane (Fig. 4C). The same behaviour has been detected for SctV-EGFP in the
233 absence of SctD (Diepold *et al*, 2011), supporting the notion that at an external pH of 4, SctV is released
234 from the SctD structure.

235

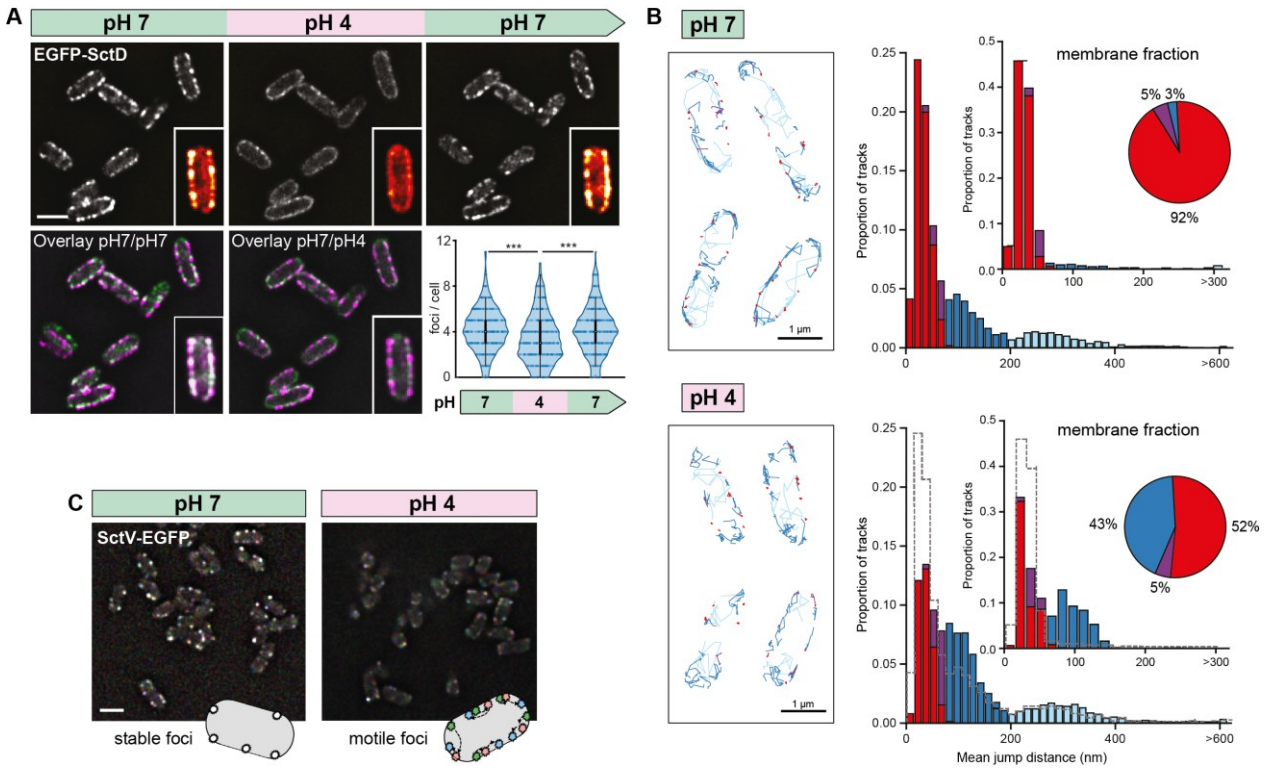

236

237 **Fig. 4 – The bitopic IM protein SctD react to low external pH**

238 (**A**) Fluorescent micrographs of EGFP-SctD in live *Y. enterocolitica*, consecutively subjected to different external
239 pH in a flow cell. Images were taken under secreting conditions, 10 minutes after bacteria were subjected to the
240 indicated pH. Insets, enlarged single bacteria, visualized with the ImageJ red-hot color scale. Bottom, overlays of
241 fluorescence at pH 7 before pH change (magenta) and pH 7 after pH change or pH 4 (green). Bottom right,
242 quantification of foci per bacterium. *n* = 1384-1709 foci in 408 cells per condition from a representative
243 experiment. (**B**) PAmCherry-SctD dynamics in exemplary living *Y. enterocolitica* (left) and histograms (right) of
244 the mean jump distances (MJD) of PAmCherry-SctD trajectories weighted by the number of jump distances
245 (# JDs) used for calculating each MJD. Only trajectories with more than 6 one-frame jumps are shown and
246 included into the analysis. Upper panel was measured at pH 7, lower panel at pH 4. Trajectories are assigned into
247 two diffusive states: static (red) and mobile (violet and blue fractions) based on the experimental localization
248 precision. The mobile trajectories are sorted into three MJD categories: lower than 60 nm (violet), lower than
249 195 nm (dark blue) and higher than 195 nm (light blue). Counts were normalized to the total number of
250 trajectories. At pH 7 we acquired 29,859 trajectories (60% static, 2% mobile below 60 nm MJD, 25% mobile from
251 60 to 195 nm MJD, 13% mobile faster than 195 nm MJD; 19,473 membrane-bound trajectories). At pH 4 we

252 acquired 33,036 trajectories (34% static, 4% mobile below 60 nm MJD, 44% mobile from 60 to 195 nm MJD, 18%
253 mobile faster than 195 nm MJD; 21,600 membrane-bound trajectories). The bin size of 15 nm was calculated
254 using the Freedman-Diaconis rule. The inset histograms display the statistics of only membrane-bound
255 trajectories. Pie plots display the percentage of each MJD category to the total number of membrane-bound
256 trajectories. The number of trajectories of membrane-bound static PAmCherry-SctD molecules decreases in pH
257 4 (92% to 52%), while the number of diffusing PAmCherry-SctD with MJDs lower than 195 nm (dark blue bars)
258 increases (3% to 43%). The fast fractions of PAmCherry-SctD molecules of MJDs higher than 195 nm (light blue),
259 which are only visible for the whole cell analysis, remain constant. The grey dashed lines in the pH 4 panels
260 represent the outlines of the pH 7 analysis. (**C**) Spatial stability of SctV-EGFP foci over time at the indicated
261 external pH. Three images of the same focal plane were taken at 10 s intervals. The green channel shows the cell
262 at t = 0 s, the blue channel at t = 10 s, and the red channel at t = 20 s. Scale bars, 2 µm.

263

264 Physiological advantage of temporary suppression of type III secretion at low pH

265 We reasoned that bacteria could benefit from the dissociation of the cytosolic T3SS components at low
266 external pH to suppress secretion in the stomach, where pH values of 4 and below prevail, which might
267 lead to energy depletion or even elicit immune reactions. If this would indeed be the case, bacteria
268 with a similar infection route, but not bacteria that do not pass through the stomach during normal
269 infection, and therefore are not under evolutionary pressure to suppress T3SS activity at low pH, would
270 be expected to display the same pH dependence for the localization of cytosolic T3SS components. We
271 therefore tested the localization of cytosolic components at low external pH in *Shigella flexneri* and
272 *Pseudomonas aeruginosa*. *S. flexneri* is a gastrointestinal pathogen that uses an evolutionarily distant
273 T3SS, but like *Y. enterocolitica*, needs to pass the stomach to invade the colonic and rectal epithelium.
274 In contrast, the T3SS of *Y. enterocolitica* and *P. aeruginosa* are closely related (Abby & Rocha, 2012),
275 but the infection strategies of the two species differ. *P. aeruginosa* is not a gastrointestinal pathogen
276 and mainly enters the host body through wounds. In agreement with the hypothesis that the
277 dissociation of cytosolic components at low external pH is a conserved adaptation to the passage of
278 low pH parts of the gastrointestinal system during a normal infection, the fraction of *S. flexneri* GFP-
279 SctN cells (Burgess *et al*, 2020) with foci decreased at pH 4, whereas this was not the case for *P.*
280 *aeruginosa* EGFP-SctQ cells (Fig. 5, Suppl. Fig. 12).

281

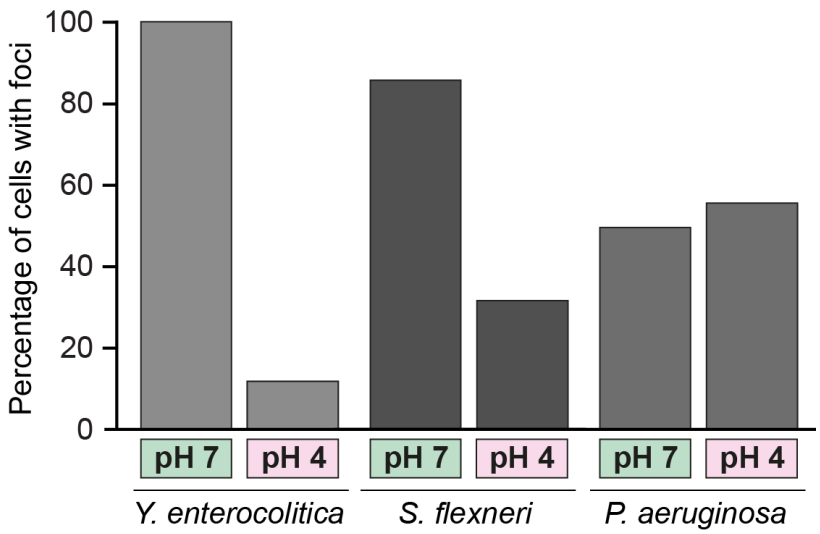

Fig. 5 – The effect of external pH on the assembly of cytosolic T3SS components is species-specific

Percentage of bacteria with fluorescent foci at the indicated external pH for *Yersinia enterocolitica EGFP-SctQ, Shigella flexneri GFP-SctN,* and *Pseudomonas aeruginosa EGFP-SctQ*, respectively. *n* = 246, 472, 164, 277, 155, 182 bacteria from at least 10 fields of view per condition.

To determine a potential molecular mechanism for this effect, we identified amino acids in the periplasmic domain of SctD that could be protonated at pH 4, but not at pH 7 (Asp, Glu, His), and focused on the subset of these amino acids that differ between *Y. enterocolitica* and *P. aeruginosa* (Suppl. Fig. 13). However, single amino acid substitutions, as well as the combination of all four substitutions still led to dissociation of the cytosolic component SctQ, as well as a loss of secretion at pH 4 (Suppl. Fig. 14) suggesting that the effect of the pH might not be conveyed by discrete salt bridges.

After the passage of the stomach, *Y. enterocolitica* arrive in the pH-neutral intestine, where they pass the M cells across the intestinal epithelium. At this point, the injectisome must be ready to manipulate immune cells. To test whether the reversible dissociation of the cytosolic T3SS components supports a fast activation of the T3SS once back at neutral pH, we monitored protein secretion over time after a temporary drop of external pH to 4. We found that secretion was suppressed at low pH, but recovered within the first hour after reaching neutral pH (Fig. 6A). Notably, this recovery is much faster than the onset of effector secretion after *de novo* assembly of the T3SS by a temperature change to 37°C (Fig. 6A), supporting the notion that bacteria benefit from the temporary dissociation of the cytosolic subunits at low pH in two ways: This mechanism suppresses protein secretion at low external pH, while ensuring a fast reactivation upon reaching a pH-neutral environment (Fig. 6B).

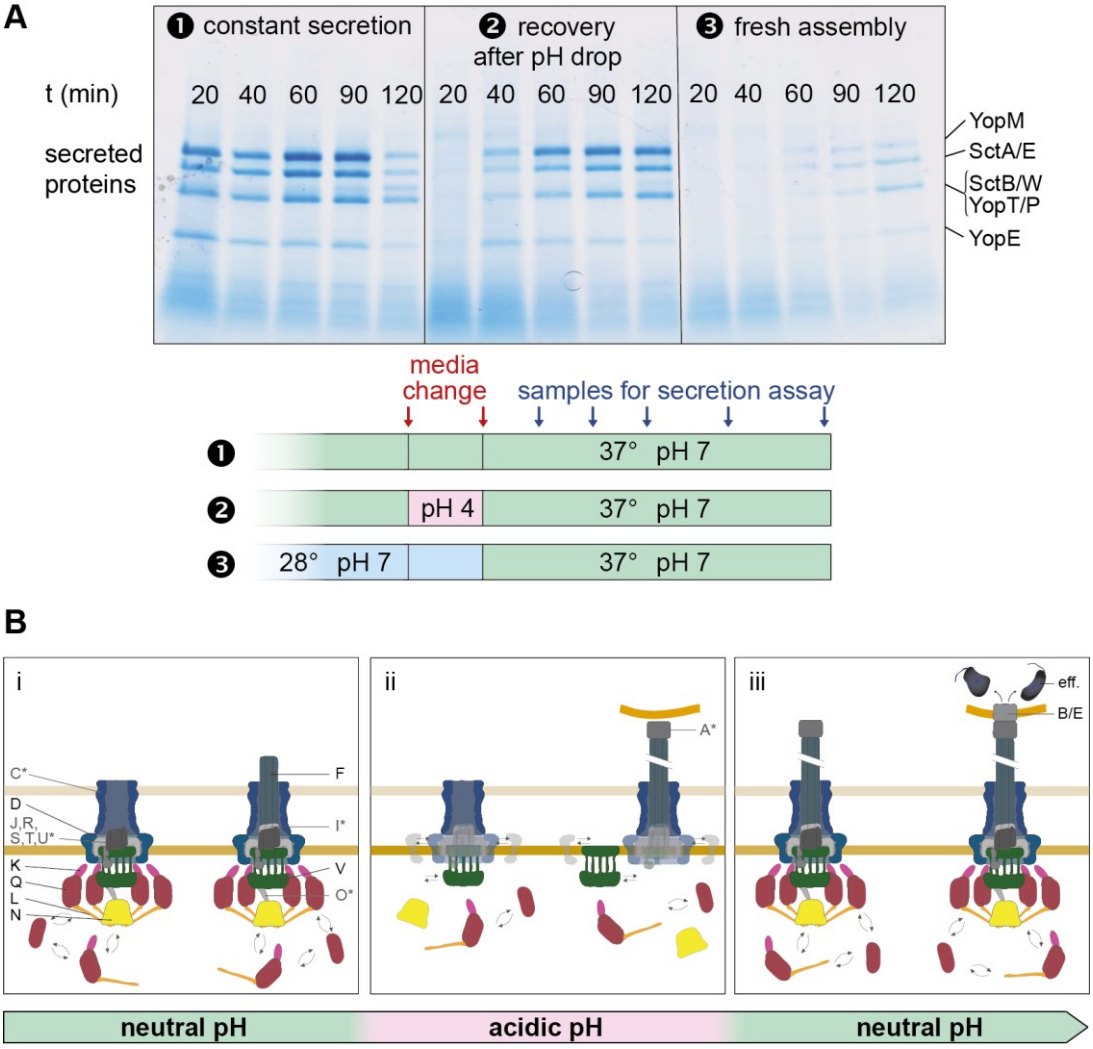

Fig. 6 – Temporary suppression of T3SS activity at low external pH enables a fast re-activation of secretion

(**A**) *In vitro* secretion assay showing the proteins exported by the T3SS in *Y. enterocolitica* MRS40 at the given time points after the second media change, (1) under constantly secretion-inducing conditions, (2) after a temporary change of the external pH to 4, (3) after incubation at 28°C, where no injectisomes are assembled. Right side, exported effectors, based on (Iriarte & Cornelis, 1998; Diepold *et al*, 2012). (**B**) Model of the pH-dependent suppression of T3SS activity. From left to right: (i) Assembly of the T3SS upon entry into host organisms; cytosolic components bound and exchanging with cytosolic pool. (ii) Prevention of effector translocation upon host cell attachment in the stomach, because cytosolic components are exclusively cytosolic. (iii) Re-association of cytosolic components to the injectisome and effector translocation upon host cell contact in neutral body parts. Letters represent protein identifiers (common Sct nomenclature); eff., effectors. Proteins whose localization was not specifically tested are indicated by asterisks and grey font. Straight double arrows indicate diffusion in membrane; curved double arrows indicate exchange of cytosolic subunits or subcomplexes between the cytosolic and the injectisome-bound state.

327 Discussion

328 On their way through the gastrointestinal system, bacteria encounter a multitude of different pH
329 environments. Importantly, the highly acidic stomach acts as natural barrier for food-borne infections.
330 Gastrointestinal pathogens express factors that facilitate survival in these conditions, such as urease,
331 of which high amounts are exported in *Y. enterocolitica* (Young *et al*, 1996; Hu *et al*, 2009; Heroven &
332 Dersch, 2014; Chen *et al*, 2016; Stingl & De Reuse, 2005). It was not known, however, if and how the
333 activity of the T3SS, an essential virulence factor for many gastrointestinal pathogens, is regulated
334 under these conditions. Although the T3SS target cells are downstream of the stomach for most
335 gastrointestinal pathogens, cells in the gastric mucosa can be accessible and bacteria can attach to host
336 cells at low pH (Fig. 1B, Suppl. Videos 1-2). Our data support the notion that bacteria prevent premature
337 injection into host cells at this stage by directly using the external pH as a cue for the temporary
338 suppression of the T3SS. While parts of the T3SS, including the needle, remain stable, the cytosolic
339 components dissociate from the injectisome in an acidic environment (pH 4 and below). This effect
340 persists at low external pH; however, once the bacteria encounter neutral external pH, both adherence
341 via the adhesin YadA to collagen is significantly increased (Fig. 1D), and the binding of the cytosolic
342 components is restored (Fig. 2). Bacteria conceivably benefit from this mechanism, which prevents
343 premature effector translocation into any eukaryotic cells in contact in the acidic regions of the
344 stomach, an event that would be energetically expensive and might elicit immune responses. Once the
345 pH-neutral intestine is reached, secretion is restarted within 20-40 minutes, which is significantly faster
346 than *de novo* synthesis of injectisomes at this time (Fig. 6).

347 We found that similarly to *E. coli* (Slonczewski *et al*, 1981; Krulwich *et al*, 2011), *Y. enterocolitica* can
348 partially compensate for acidic external environment, and that at an external pH of 4.0, the cytosolic
349 pH remained at 6.3-6.4 (Fig. 3A). When we used a proton ionophore to create this cytosolic pH at a
350 similar external pH, the cytosolic T3SS components remained bound to the injectisome (Fig. 3B),
351 suggesting that the external pH is sensed outside the bacterial cytosol. A central open question is how
352 exactly the pH change is sensed in the extracytosolic space. A prime candidate to be involved is the
353 bitopic IM component SctD, which could react to a drop in external pH with its periplasmic domain and
354 then transmit this signal to the cytosol. Indeed, our data show that the localization of SctD within the
355 membrane clearly differs between external pH of 7 and 4 (Fig. 4). Interestingly, SctD is one of the least
356 conserved genes in the T3SS, especially in comparison to its direct structural neighbors, the highly
357 conserved SctC secretin ring in the OM, as well as SctJ and the export apparatus proteins in the IM
358 (Diepold & Wagner, 2014). While this low sequence similarity prevented a multi-sequence alignment
359 to identify conserved differences between the T3SS of gastrointestinal and non-gastrointestinal

360 pathogens (except for the closely related *Y. enterocolitica* and *P. aeruginosa*, Suppl. Fig. 12B), it
361 supports the notion that SctD is involved in species-specific adaptation of the T3SS, such as pH sensing.
362 This hypothesis is further substantiated by the finding that in *P. aeruginosa*, which does not pass the
363 stomach during a normal infection, the effect of low pH is significantly restricted, with the majority of
364 EGFP-SctQ foci remaining present at low external pH (Fig. 5). The single or combined mutation of the
365 amino acids in *Y. enterocolitica* SctD that differ from the *P. aeruginosa* homolog and are expected to
366 be protonated at pH 4, but not at pH 7 (histidines 193, 205, 353, 376) to neutral amino acids did not
367 phenocopy the lack of pH sensitivity, suggesting that a broader reversible conformational change at
368 low pH is responsible for the observed effect. This could include the disruption of intermolecular
369 interaction interfaces within or between SctD and the secretin ring SctC. Due to the periplasmic location
370 of any possible fusion protein, SctC could not be directly visualized in this study; however, given the
371 high stability of secretin rings (Rappl *et al*, 2003; Burghout *et al*, 2004; Majewski *et al*, 2018) the
372 interfaces between SctC and SctD, or between neighboring SctD molecules are prime candidates for a
373 pH-dependent temporary dissociation.

374 Both possible types of pH sensing, direct structural change and rearrangement of intermolecular
375 interactions, are used by biological systems: The *E. coli* membrane-integrated transcriptional regulator
376 CadC senses acidic pH through direct protonation of a charged surface patch in its C-terminal
377 periplasmic domain, and transduces the signal to the cytosol by its N-terminal cytosolic domain
378 (Haneburger *et al*, 2011). Similarly, the *P. syringae* T3SS effector AvrPto transitions from a largely
379 unfolded state in the mildly acidic bacterial cytosol to a well-defined fold in the neutral host cytosol
380 (Dawson *et al*, 2009). Perhaps most strikingly, the highly ordered multimeric structures of
381 bacteriophages undergo large-scale structural changes at low pH, that are reversible (Helenius *et al*,
382 1980; Mauracher *et al*, 1991; Taylor *et al*, 2002). Indeed, our data indicate a reversible partial
383 delocalization of SctD at low external pH (Fig. 4). The presence of SctD is required for binding of any
384 cytosolic T3SS component (Diepold *et al*, 2010, 2017), most likely through a direct contact of four SctD
385 to one SctK at the cytosolic interface of the IM (Hu *et al*, 2017), indicating that this partial displacement
386 of SctD (Fig. 4) is causal for the dissociation of the cytosolic T3SS components.

387 The dissociation kinetics of the cytosolic components of the T3SS revealed a dissociation half-time of
388 about one to two minutes under secreting conditions (Fig. 2D, Suppl. Video 3). This value is strikingly
389 similar to the exchange rate of SctQ at the injectisome (Diepold *et al*, 2015), suggesting that at low
390 external pH, primarily the re-association of the cytosolic components is prevented. This adaptation of
391 T3SS function may explain the so-far enigmatic benefit of the observed dynamics of the cytosolic parts
392 of the injectisome during its function. Notably, the observed dissociation of the cytosolic proteins in

393 response to low external pH may not reveal the complete mechanism for suppression of T3SS activity
394 at this pH. The observation that the dissociation of the cytosolic components occurs at a slightly lower
395 pH than the loss of effector secretion, and that the re-initiation of secretion occurs later than the initial
396 recovery of foci indicates that other factors might participate in this phenotype. The slightly delayed
397 activation of secretion after restoration of neutral pH could also be explained by the time required for
398 re-associating SctV to the machinery (the cytosolic components can already bind to the membrane
399 rings in the absence of SctV (Diepold *et al*, 2010)). This delay may, in fact, be beneficial for *Y.*
400 *enterocolitica*, as it delays the antiphagocytic effects of the T3SS effectors, which otherwise may
401 hamper the passage of *Y. enterocolitica* through the M cells that is required to access the lymphoid
402 follicles of the Peyer's patches (Cornelis, 2002).

403 Like the *Y. enterocolitica* T3SS, the intracellular *Salmonella enterica* SPI-2 T3SS is strongly influenced by
404 the external pH; however, the mechanism described for SPI-2 differs from the one described in this
405 study. Injectisome assembly and secretion of the translocon components in SPI-2 are activated by the
406 low pH of the surrounding vacuole (around pH 5.0) (Rappl *et al*, 2003; Yu *et al*, 2010). After this step,
407 neutral pH, most likely indicative of a successfully established connection to the neutral host cytosol,
408 leads to the disassembly of a gatekeeper complex, which in turn licenses the translocation of effectors
409 (Yu *et al*, 2010). Strikingly, a single amino acid exchange in the export apparatus protein SctV governs
410 this pH-dependent effect (Yu *et al*, 2018). Both the sensory and the functional connection between the
411 pH and T3SS activity differ between *Salmonella* SPI-2 and *Y. enterocolitica*, which highlights the high
412 degree of functional adaptability of the T3SS.

413 In this study, we found that dynamic exchange of cytosolic components of the T3SS enables to suppress
414 the premature activation of the T3SS at low external pH in *Y. enterocolitica*. Strikingly, this effect is
415 conserved in *S. flexneri* and very likely in other gastrointestinal pathogens, but not in *P. aeruginosa*,
416 which does not pass low pH regions during normal infections. Our data highlight that not only the
417 effector repertoire, but also dynamics and function of T3SS are adapted to the specific environment of
418 the respective bacteria. This newly described pathway is a striking showcase for the variety and
419 sophistication of mechanisms that allow bacteria to use different aspects of T3SS assembly and
420 function, including protein dynamics, to tailor the activity of this essential virulence mechanism to their
421 specific needs during infection.

422

423

424 Material and Methods

425 *Bacterial strain generation and genetic constructs*

426 A list of strains and plasmids used in this study can be found in Supplementary Table 1. The
427 *Y. enterocolitica* strains used in this study are based on the *Y. enterocolitica* wild-type strain MRS40
428 (Sory *et al*, 1995), and the strain IML421asd (ΔHOPEMTasd), in which all major virulence effector
429 proteins (YopH,O,P,E,M,T) are deleted (Kudryashev *et al*, 2013). Furthermore, this strain harbors a
430 deletion of the aspartate-beta-semialdehyde dehydrogenase gene which render the strain auxotrophic
431 for diaminopimelic acid (DAP).

432 Unless stated otherwise, all fusion proteins used were expressed as endogenous fusions from their
433 native location on the pYV virulence plasmid, which were introduced by two step homologous
434 recombination (Kaniga *et al*, 1991).

435 For cloning and conjugation the *E. coli* strains Top10 and SM10 λpir were used, respectively. All
436 constructs were confirmed by sequencing (Eurofins Scientific). Constructs with single amino acid
437 substitutions in SctD or SctF were created by overlapping PCR using Phusion polymerase (New England
438 Biolabs), and expressed from an arabinose controlled expression vector (pBAD).

439 *Bacterial cultivation, in vitro secretion assays and fluorescence microscopy*

440 *Y. enterocolitica* day cultures were inoculated from stationary overnight cultures to an OD_{600} of 0.15
441 and 0.12 for secreting and non-secreting conditions, respectively, in BHI medium (Suppl. Table 2)
442 supplemented with nalidixic acid (35 mg/ml), diaminopimelic acid (80 mg/ml), glycerol (0.4%) and
443 $MgCl_2$ (20 mM). Where required, ampicillin was added (0.2 mg/ml) to select for pBAD-based plasmids.
444 For secreting conditions, cultures were additionally supplemented with 5 mM EGTA; for non-secreting
445 conditions, cultures were additionally supplemented with 5 mM $CaCl_2$ and filtered through a 0.45 µm
446 filter. Cultures were incubated at 28°C for 90 minutes. At this time point, expression of the *yop* regulon
447 was induced by a rapid temperature shift to 37°C in a water bath and expression of proteins *in trans*
448 was induced by addition of 0.2-1.0% arabinose, as indicated.

449 For effector visualization or total cell analysis, bacteria were incubated at 37°C between 1-3 hours, as
450 indicated. 2 ml of the culture were collected at 21,000 *g* for 10 min. The supernatant was separated
451 from the total cell fraction and precipitated with trichloroacetic acid (TCA) for 1-8 h at 4°C; proteins
452 were collected by centrifugation for 15-20 min at 21,000 *g* and 4°C, washed once with ice cold acetone
453 and then resuspended and normalized in SDS-PAGE loading buffer. Total cell samples were normalized
454 to $2.5x10^8$ bacteria and supernatant samples to the equivalent of $3x10^8$ bacteria per SDS-PAGE gel lane.

455 Samples were incubated for 5 minutes at 99°C, separated on 12-20% SDS-PAGE gels, and stained with
456 Instant blue (Expedeon).

457 For fluorescence microscopy, bacteria were treated as described above. After 2-3 h at 37°C, 400 µl of
458 bacterial culture were collected by centrifugation (2,400 *g*, 2 min) and resuspended in 200µl
459 microscopy minimal medium (Suppl. Table 2). Cells were spotted on 1.5% low melting agarose pads
460 (Sigma) in microscopy minimal medium in glass depression slides. Where required, 80 mg/ml DAP for
461 ΔHOPEMTasd-based strains, 0.2-1.0% L-arabinose for induction of *in trans* expression, 5 mM Ca^{2+} for
462 non-secreting conditions, or 5 mM EGTA for secreting conditions were added.

463 *P. aeruginosa o*vernight cultures were grown at 28°C. For secreting cultures, LB broth (Suppl. Table 2)
464 was supplemented with 20 mM $MgCl_2$, 200mM NaCl and 5 mM EGTA and inoculated to an OD_{600} of
465 0.15 and incubated for 2 h at 37°C. This culture was then used to inoculate a fresh culture containing
466 the same supplements to an OD_{600} of 0.15. Microscopy experiments were then performed 2 h later on
467 a minimal media agar pad and in LB medium.

468 *S. flexneri* over night cultures where inoculated from a fresh LB-agar plate into BHI broth. On the next
469 day, fresh BHI cultures were inoculated to an OD of 0.12 and grown to an OD of around 1 at 37°C
470 (Burgess *et al*, 2020). 1 ml of bacterial culture was collected by centrifugation (2,400 *g*, 2 min) and
471 resuspended in 100µl microscopy minimal medium (Suppl. Table 2) at the indicated pH. 2 µl of the
472 resuspension were spotted on a minimal medium agar pad adjusted to the indicated pH and then
473 visualized.

474 *Wide field fluorescence microscopy*

475 Microscopy was performed on a Deltavision Elite Optical Sectioning Microscope (Applied Precision),
476 equipped with a UApo N 100x/1.49 oil TIRF UIS2 objective (Olympus) and a UPlanSApo 100x/1.40 oil
477 objective (Olympus), using an Evolve EMCCD Camera (Photometrics). Samples were illuminated for 0.1 s
478 with a 488 nm laser with a TIRF depth setting of 3440 (TIRF) or for 0.2 s with green LED light (standard
479 oil objective). Excitation and emission filter sets used were 475/28 and 525/48 nm (green), 575/25 and
480 625/45 nm (red), or 632/22 and 679/34 nm (Cy5). The micrographs where deconvolved using softWoRx
481 7.0.0 (standard "conservative" settings). Images were then further processed with ImageJ-Fiji. Where
482 necessary, drift correction was performed with the StackReg Plugin. For figures, representative fields
483 of view were selected, and brightness and contrast of the micrographs was adjusted identically within
484 compared images.

485 Samples sizes and number of replicates for wide field microscopy and all other experiments were
486 determined prior to the experiments, based on experimental feasibility and their potential to draw
487 clear conclusions. These numbers were not changed based on the experimental outcome.

488 *Flow cell based TIRF microscopy*

489 A microscopy flow cell was manufactured based on (Berg & Block, 1984). Formation of injectisomes
490 was induced under non-secreting conditions. After formation of the injectisomes, bacteria were
491 collected and resuspended in approximately 0.5 volumes of microscopy medium supplemented with
492 80 mg/ml DAP and 5mM EGTA. The flow cell was pre-incubated with microscopy medium and a bottom
493 coverslip (25 mm No. 1.5; VWR) was attached to the cell. Bacteria were spotted on the coverslip and
494 incubated for 1 min to allow attachment to the glass surface. The cover slip was covered with 60 µl of
495 minimal medium and sealed from the top with an additional cover slip. The flow cell was mounted on
496 the microscopy stage and gravity-driven buffer flow in the chamber was induced using a 1 ml syringe.
497 To exchange the buffer in the flow cell, the tube was quickly relocated to the new buffer. Complete
498 buffer exchange in the flow cell was determined to take 39 $\pm$ 5 s (n = 7).

499 *Detection and quantification of fluorescent foci*

500 Detection and quantification of foci was performed by first segmenting the images using the software
501 BiofilmQ. After segmentation, we fluorescent foci were detected within BiofilmQ. The foci were filtered
502 by their intensity above the background intensity of the cell, calculated by subtracting a blurred image.

503 *Maleimide based needle staining*

504 To visualize the injectisome needles, expression of $SctF_{S5C}$ (Milne-Davies *et al*, 2019) was induced from
505 plasmid. Protein expression was induced with 0.4-1.0% L-arabinose at the temperature shift. After 2-3
506 h, bacteria were collected and resuspended in 0.2 volumes of microscopy medium supplemented with
507 5 µM of a CF^{TM}488A/633 maleimide dye (Sigma-Aldrich, USA) for 5 min in 100 µl of minimal medium at
508 37°C. After staining, cells were washed once with 500 µl of minimal medium and spotted on 1.5%
509 agarose pads in the same medium.

510 *Halo staining with Janelia fluorescent dyes*

511 To stain and visualize a defined pool of T3SS proteins, Halo-labeled proteins were visualized using
512 Janelia Fluor 549-NHS ester and Janelia Fluor 646-NHS ester. 500 µl of bacterial culture were collected
513 by centrifugation (2,400 *g*, 2 min) and resuspended in 100 µl microscopy medium. Bacteria were
514 stained with 0.2 µM Janelia Fluor JF-646/JF-549 dyes at 37°C for 30 min in a tabletop shaker.

515 Afterwards, bacteria were washed twice in 500 µl minimal medium and then visulaized in a flow cell or
516 on 1.5% agarose pads in the same medium.

517 *Equilibration of cytosolic and external pH*

518 2,4-dinitrophenol (DNP) was diluted in methanol and used at a final concentration of 2 mM in
519 microscopy minimal medium. Cells were grown as described above, and resuspended in DNP
520 containing medium immediately before being spotted on 1.5% agarose pads in the same medium
521 containing DNP.

522 *Bacterial survival test*

523 Wild-type MRS40 *Y. enterocolitica* were inoculated to an OD_{600} of 0.12 in non-secreting conditions and
524 incubated for 1.5 h at 28°C to reach exponential growth phase. Cells were collected by centrifugation
525 at 2,400 *g* for 2 min. The supernatant was discarded and the collected bacteria were resuspended in a
526 range of pH-adjusted media buffered with 50 mM glycine, 50 mM HEPES and 50 mM MES. These
527 cultures were incubated for 15 min at 28°C and afterwards a dilution series in neutral media was
528 performed. For the visualization, 4 µl of bacterial suspension were spotted on a neutral LB agar
529 supplemented with nalidixic acid and incubated at 28°C overnight.

530 *Growth curve assays*

531 Wild-type *Y. enterocolitica* MRS40 were inoculated to an OD_{600} of 0.12 in secreting conditions and
532 incubated for 90 min at 28°C. At this point, cells where collected by centrifugation (2,400 *g*, 2 min), and
533 resuspended in 37°C fresh pre-warmed secreting medium buffered with 50 mM glycine, 50 mM HEPES
534 and adjusted to the indicated pH. After 90 min, one batch of cells incubated at pH 4 were collected
535 again and resuspended in fresh buffered secretion medium at pH 7. All strains were incubated for
536 further 90 min. During the experiment, the OD_{600} was measured every 30 min in technical duplicates.

537 *pHluorin purification and calibration*

538 The protocol described by Nakamura et al. (Nakamura *et al*, 2009) was adapted for bench top
539 purification. Expression of ratiometric GST-pHluorin$_{M153R}$ in *E. coli* DH5αZI was induced in a 500 ml
540 culture with 1 mM IPTG, followed by 4 h incubation at 28°C. Cells were harvested and stored for further
541 processing at -80°C. Next, cells were thawed on ice, resuspended in lysis buffer and disrupted by two
542 passages through a French Press. The lysate was centrifuged (25,000 rpm, 60 min, 4°C) and the
543 supernatant was gently mixed with the previously equilibrated glutathione agarose at 4°C for 1.5 h in
544 a small spinning wheel. The agarose was collected by centrifugation (500 *g*, 5 min) and washed with
545 PBS three times. A thrombin digest was performed in 2 ml PBS while incubating for 60 min on a roll

546 mill. Agarose was removed by centrifugation (500 *g*, 5 min) and the protein was stored at -80°C for
547 further use.

548 The calibration was performed on a Deltavision Elite microscope. 5 µl of purified pHluorin protein were
549 spotted on a KOH-cleaned microscopy slide in an enclosed compartment (Thermo Fisher Scientific
550 GeneFrame, AB-0577) and incubated for 5 min to ensure attachment to the glass surface. Then, 10 µl
551 of pH-adjusted PBS buffered with 200 mM glycine, 200 mM HEPES, and 200 mM MES were added.
552 Ratiometric pHluorin fluorescence was determined using the DAPI excitation filter (390/18nm) or GFP
553 excitation filter (475/28nm) at 32% illumination intensity, in combination with a GFP emission filter set
554 (525/48nm) with 0.3 s exposure time. The overall fluorescence of the images before deconvolution was
555 determined and corrected for background fluorescence levels, which were measured with an empty
556 slide filled with PBS. The ratio of DAPI/Green vs Green/Green fluorescence was determined for a pH
557 range from pH 8 – pH 5 in 0.5 pH steps.

558 *Single particle tracking photoactivated localization microscopy (sptPALM)*

559 Bacteria were cultivated under non-secreting conditions as described above. After 2.5 h of incubation
560 at 37°C, the media was changed to pre-warmed (37°C) minimal microscopy medium containing the
561 same supplements as the BHI before. Cells were incubated for 30 min and then washed four times in 5
562 volumes of pre-warmed (37°C) EZ medium (Supplementary Table 2) supplemented with DAP and 5 mM
563 $CaCl_2$. Bacteria were concentrated 2x after the last wash and spotted on a 1.5% agarose pad in EZ
564 medium supplemented with DAP and 5 mM $CaCl_2$ on a KOH-cleaned microscopy slide in an enclosed
565 compartment (Thermo Fisher Scientific GeneFrame, AB-0577). Imaging was performed on a custom
566 build setup based on an automated Nikon Ti Eclipse microscope equipped with appropriate dichroic
567 and filters (ET DAPI/FITC/Cy3 dichroic, ZT405/488/561rpc rejection filter, ET610/75 bandpass,
568 Chroma), and a CFI Apo TIRF 100x oil objective (NA 1.49, Nikon). All lasers (405 nm OBIS, 561 nm OBIS;
569 all Coherent Inc. USA) were modulated via an acousto-optical tunable filter (AOTF) (Gooch and
570 Housego, USA). Fluorescence was detected by an EMCCD camera (iXON Ultra 888, Andor, UK) in frame
571 transfer mode and read-out parameter settings of EM-gain 300, pre-amp gain 2 and 30 MHz read-out
572 speed. The z-focus was controlled using a commercial perfect focus system (Nikon). Acquisitions were
573 controlled by a customized version of Micro-Manager (Edelstein *et al*, 2010). Live cell sptPALM
574 experiments were performed on a customized heating stage at 25°C. Live *Y. enterocolitica* PAmCherry-
575 SctD cells were imaged in HILO illumination mode (Tokunaga *et al*, 2008). Applied laser intensities
576 measured after objective were 35 W/cm^2 (405 nm) and 800 W/cm^2 (561 nm). Prior to recording each
577 new region of interest (ROI), a pre-bleaching step of 561 nm illumination was applied for 30 seconds to
578 reduce autofluorescence. Videos were then recorded for 2000 frames pulsing the 405 nm laser every

579 20th imaging frame at 5 Hz with an exposure time of 200 ms per frame. After sptPALM imaging, a bright
580 light snapshot of all illuminated regions was recorded to obtain the bacterial cell shapes.

581 Single molecule localizations were obtained using *rapidSTORM* 3.3.1 (Wolter *et al*, 2012) and single
582 cells were manually segmented in *Fiji (ImageJ 1.51f)* (Schindelin *et al*, 2012). sptPALM data was tracked,
583 visualized and filtered using a customized tracking software written in C++ (***swift***, unpublished
584 software, RG Endesfelder). Trajectories were allowed to have a maximum of 5 frames of gap time (e.g.
585 caused by fluorophore blinking). Trajectories were assigned to their diffusive states (static and mobile)
586 on the basis of the experimental localization precision of about 25 nm (determined by the NeNA
587 method (Endesfelder *et al*, 2014). For trajectories with more than 6 one-frame jumps, the mean jump
588 distance (MJD) was calculated (jumps spanning several frames due to dark times were not used in MJD
589 calculations). The obtained MJDs were weighted by the number of jumps and displayed in a histogram
590 using OriginPro 9.4 (Origin LAB Corporation, USA).

591 *Y. enterocolitica YadA and cellular adhesion assays*

592 To measure YadA adhesion to collagen at different pH values, an ELISA-like binding assay was
593 performed (Leo *et al*, 2008, 2010; Saragliadis & Linke, 2019). Clear 96 well plates (Sarstedt, Ref.
594 82.1581) were coated with 100 µl of calf collagen type I (10 µg/ml, ThermoFisher A1064401) in H_2O
595 with 0.01 M acetic acid for 1h at room temperature (RT). The supernatant was discarded and the wells
596 were blocked with 1% BSA in PBS and afterwards washed three times with 0.1% BSA in PBS. Afterwards,
597 100 µL of purified YadA head domains with a C-terminal His_6-tag at a concentration of 10 µg/mL were
598 incubated in the wells. In order to test binding at different pH, the YadA heads were diluted in acetic
599 acid/sodium acetate at pH 4.0 or pH 5.0 and for higher pH values in PBS at pH 6.0 and 7.0. Binding was
600 allowed for 1 h at RT. Afterwards, the plate was emptied and washed three times with 0.1% BSA in PBS.
601 The wells were blocked with 1.0% BSA in PBS for 1h at RT. For detection, Ni-HRP conjugates (HisProbe-
602 HRP, Thermo Fisher Scientific, Ref. 15165) were diluted in 0.1% BSA in PBS and 100 µl per well were
603 incubated for 1 h at RT. The Ni-HRP conjugate solution was discarded and the wells washed three times
604 with PBS. Detection was performed using ABTS substrate (Thermo Scientific. Ref. 34026). Development
605 was allowed for 30 min. Absorption was measured at 405 nm on a plate reader (Biotek Synergy H1).

606 Glass binding assays for live *Y. enterocolitica* were performed in a flow cell. Bacteria were treated as
607 mentioned above, resuspended in microscopy medium at the indicated pH value, and added to the
608 flow cell as described above. Bacteria were tracked visually for 10 min afterwards.

609

610

611 Acknowledgements

612 We thank Nicholas Dickenson (Utah State University, Logan, USA) for the kind sharing of *Shigella*
613 *flexneri* GFP-Spa47, Sophie Bleves (Aix-Marseille Univeristy, FR) for the *Pseudomonas aeruginosa* PAO1
614 strain, Marc Erhardt (Humboldt University Berlin, Germany), Tohru Minamino (Osaka University,
615 Japan), and Gero Miesenböck (University of Oxford, UK) for the pHluorin$_{M153R}$ DNA, Luke Lavis (Janelia
616 Research Campus, USA) for the kind donation of Janelia Fluor dyes, and Malte Buchholz (University of
617 Marburg, Germany) for helpful discussions about gastrointestinal infection pathways.

618 This work was supported by the Max Planck Society. It was also funded by the Horizon 2020 Innovative
619 Training Network "ViBrANT" (to DL).

620

621 References

622 Abby SS & Rocha EPC (2012) The non-flagellar type III secretion system evolved from the bacterial flagellum
623 and diversified into host-cell adapted systems. *PLoS Genet.* **8:** e1002983

624 Berg HC & Block SM (1984) A Miniature Flow Cell Designed for Rapid Exchange of Media Under High-power
625 Microscope Objectives. *Microbiology* **130:** 2915–2920

626 Bernal I, Börnicke J, Heidemann J, Svergun D, Horstmann JA, Erhardt M, Tuukkanen A, Uetrecht C & Kolbe
627 M (2019) Molecular Organization of Soluble Type III Secretion System Sorting Platform Complexes. *J.*
628 *Mol. Biol.* **431:** 3787–3803

629 Burgess JL, Case HB, Burgess RA & Dickenson NE (2020) Dominant negative effects by inactive Spa47
630 mutants inhibit T3SS function and Shigella virulence. *PLoS One* **15:** e0228227

631 Burghout P, Boxtel R, Gelder P, Ringler P, Müller SA, Tommassen J & Koster M (2004) Structure and
632 electrophysiological properties of the YscC secretin from the type III secretion system of Yersinia
633 enterocolitica. *J. Bacteriol.* **186:** 4645–4654

634 Büttner D (2012) Protein export according to schedule: architecture, assembly, and regulation of type III
635 secretion systems from plant- and animal-pathogenic bacteria. *Microbiol. Mol. Biol. Rev.* **76:** 262–310

636 Chen S, Thompson KM & Francis MS (2016) Environmental Regulation of Yersinia Pathophysiology. *Front.*
637 *Cell. Infect. Microbiol.* **6:** 25

638 Clerc P, Baudry B & Sansonetti PJ (1986) Plasmid-mediated contact haemolytic activity in Shigella species:
639 correlation with penetration into HeLa cells. *Ann. Inst. Pasteur. Microbiol.* **137A:** 267–78

640 Coburn B, Sekirov I & Finlay BB (2007) Type III secretion systems and disease. *Clin. Microbiol. Rev.* **20:** 535–
641 49

642 Cornelis GR (2002) Yersinia type III secretion: Send in the effectors. *J. Cell Biol.* **158:** 401–408

643 Cornelis GR (2006) The type III secretion injectisome. *Nat. Rev. Microbiol.* **4:** 811–825

644 Dawson JE, Seckute J, De S, Schueler SA, Oswald AB & Nicholson LK (2009) Elucidation of a pH-folding switch
645 in the Pseudomonas syringae effector protein AvrPto. *Proc. Natl. Acad. Sci. U. S. A.* **106:** 8543–8

646 Dechant R, Binda M, Lee SS, Pelet S, Winderickx J & Peter M (2010) Cytosolic pH is a second messenger for
647 glucose and regulates the PKA pathway through V-ATPase. *EMBO J.* **29:** 2515–26

648 Deng W, Marshall NC, Rowland JL, McCoy JM, Worrall LJ, Santos AS, Strynadka NC & Finlay BB (2017)
649 Assembly, structure, function and regulation of type III secretion systems. *Nat. Rev. Microbiol.* **15:** 323–
650 337

651 Diepold A, Amstutz M, Abel S, Sorg I, Jenal U & Cornelis GR (2010) Deciphering the assembly of the Yersinia
652 type III secretion injectisome. *EMBO J.* **29:** 1928–1940

653 Diepold A, Kudryashev M, Delalez NJ, Berry RM & Armitage JP (2015) Composition, Formation, and
654 Regulation of the Cytosolic C-ring, a Dynamic Component of the Type III Secretion Injectisome. *PLOS*
655 *Biol.* **13:** e1002039

656 Diepold A, Sezgin E, Huseyin M, Mortimer T, Eggeling C & Armitage JP (2017) A dynamic and adaptive
657 network of cytosolic interactions governs protein export by the T3SS injectisome. *Nat. Commun.* **8:**
658 15940

659 Diepold A & Wagner S (2014) Assembly of the bacterial type III secretion machinery. *FEMS Microbiol. Rev.*
660 **38:** 802–22

661 Diepold A, Wiesand U, Amstutz M & Cornelis GR (2012) Assembly of the Yersinia injectisome: the missing
662 pieces. *Mol. Microbiol.* **85:** 878–92

663 Diepold A, Wiesand U & Cornelis GR (2011) The assembly of the export apparatus (YscR,S,T,U,V) of the
664 Yersinia type III secretion apparatus occurs independently of other structural components and involves
665 the formation of an YscV oligomer. *Mol. Microbiol.* **82:** 502–14

666 Edelstein A, Amodaj N, Hoover K, Vale R & Stuurman N (2010) Computer control of microscopes using
667 µManager. *Curr. Protoc. Mol. Biol.* **Chapter 14:** Unit14.20

668 Endesfelder U, Malkusch S, Fricke F & Heilemann M (2014) A simple method to estimate the average
669 localization precision of a single-molecule localization microscopy experiment. *Histochem. Cell Biol.*
670 **141:** 629–38

671 Evans DF, Pye G, Bramley R, Clark AG, Dyson TJ & Hardcastle JD (1988) Measurement of gastrointestinal pH
672 profiles in normal ambulant human subjects. *Gut* **29:** 1035–41

673 Grimm JB, Brown TA, English BP, Lionnet T & Lavis LD (2017) Synthesis of Janelia Fluor HaloTag and SNAP-
674 Tag Ligands and Their Use in Cellular Imaging Experiments. *Methods Mol. Biol.* **1663:** 179–188

675 Håkansson S, Schesser K, Persson C, Galyov EE, Rosqvist R, Homblé F & Wolf-Watz H (1996) The YopB protein
676 of Yersinia pseudotuberculosis is essential for the translocation of Yop effector proteins across the
677 target cell plasma membrane and displays a contact-dependent membrane disrupting activity. *EMBO*
678 *J.* **15:** 5812–5823

679 Haneburger I, Eichinger A, Skerra A & Jung K (2011) New insights into the signaling mechanism of the pH-
680 responsive, membrane-integrated transcriptional activator CadC of Escherichia coli. *J. Biol. Chem.* **286:**
681 10681–9

682 Helenius A, Kartenbeck J, Simons K & Fries E (1980) On the entry of Semliki forest virus into BHK-21 cells. *J.*
683 *Cell Biol.* **84:** 404–20

684 Heroven AK & Dersch P (2014) Coregulation of host-adapted metabolism and virulence by pathogenic
685 yersiniae. *Front. Cell. Infect. Microbiol.* **4:** 146

686 Hong JS, Hunt AG, Masters PS & Lieberman MA (1979) Requirements of acetyl phosphate for the binding
687 protein-dependent transport systems in Escherichia coli. *Proc. Natl. Acad. Sci. U. S. A.* **76:** 1213–7

688 Hu B, Lara-Tejero M, Kong Q, Galán JE & Liu J (2017) In Situ Molecular Architecture of the Salmonella Type
689 III Secretion Machine. *Cell* **168:** 1065-1074.e10

690 Hu B, Morado DR, Margolin W, Rohde JR, Arizmendi O, Picking WL, Picking WD & Liu J (2015) Visualization
691 of the type III secretion sorting platform of Shigella flexneri. *Proc. Natl. Acad. Sci.* **112:** 1047–1052

692 Hu Y, Lu P, Wang Y, Ding L, Atkinson S & Chen S (2009) OmpR positively regulates urease expression to
693 enhance acid survival of Yersinia pseudotuberculosis. *Microbiology* **155:** 2522–2531

694 Hueck CJ (1998) Type III protein secretion systems in bacterial pathogens of animals and plants. *Microbiol.*
695 *Mol. Biol. Rev.* **62:** 379–433

696 Iriarte M & Cornelis GR (1998) YopT, a new Yersinia Yop effector protein, affects the cytoskeleton of host
697 cells. *Mol. Microbiol.* **29:** 915–929

698 Jackson MW & Plano G V (2000) Interactions between type III secretion apparatus components from
699 Yersinia pestis detected using the yeast two-hybrid system. *FEMS Microbiol. Lett.* **186:** 85–90

700 Kaniga K, Delor I & Cornelis GR (1991) A wide-host-range suicide vector for improving reverse genetics in
701 Gram-negative bacteria: inactivation of the blaA gene of Yersinia enterocolitica. *Gene* **109:** 137–41

702 Keller B, Mühlenkamp M, Deuschle E, Siegfried A, Mössner S, Schade J, Griesinger T, Katava N, Braunsdorf
703 C, Fehrenbacher B, Jiménez-Soto LF, Schaller M, Haas R, Genth H, Retta SF, Meyer H, Böttcher RT, Zent
704 R, Schütz M, Autenrieth IB, et al (2015) Yersinia enterocolitica exploits different pathways to
705 accomplish adhesion and toxin injection into host cells. *Cell. Microbiol.* **17:** 1179–1204

706 Krulwich TA, Sachs G & Padan E (2011) Molecular aspects of bacterial pH sensing and homeostasis. *Nat. Rev.*
707 *Microbiol.* **9:** 330–343

708 Kudryashev M, Stenta M, Schmelz S, Amstutz M, Wiesand U, Castaño-Díez D, Degiacomi MTM, Münnich S,
709 Bleck CKC, Kowal J, Diepold A, Heinz DWD, Dal Peraro M, Cornelis GR & Stahlberg H (2013) In situ
710 structural analysis of the Yersinia enterocolitica injectisome. *Elife* **2:** e00792

711 Lara-Tejero M, Kato J, Wagner S, Liu X & Galán JE (2011) A Sorting Platform Determines the Order of Protein
712 Secretion in Bacterial Type III Systems. *Science (80-.).* **331:** 1188–91

713 Leo JC, Elovaara H, Bihan D, Pugh N, Kilpinen SK, Raynal N, Skurnik M, Farndale RW & Goldman A (2010)
714 First analysis of a bacterial collagen-binding protein with collagen toolkits: Promiscuous binding of
715 YadA to collagens may explain how YadA interferes with host processes. *Infect. Immun.* **78:** 3226–3236

716 Leo JC, Elovaara H, Brodsky B, Skurnik M & Goldman A (2008) The Yersinia adhesin YadA binds to a
717 collagenous triple-helical conformation but without sequence specificity. *Protein Eng. Des. Sel.* **21:**
718 475–484

719 Leo JC, Oberhettinger P, Schütz M & Linke D (2015) The inverse autotransporter family: intimin, invasin and
720 related proteins. *Int. J. Med. Microbiol.* **305:** 276–82

721 Majewski DD, Worrall LJ & Strynadka NC (2018) Secretins revealed: structural insights into the giant gated
722 outer membrane portals of bacteria. *Curr. Opin. Struct. Biol.* **51:** 61–72

723 Makino F, Shen D, Kajimura N, Kawamoto A, Pissaridou P, Oswin H, Pain M, Murillo I, Namba K & Blocker AJ
724 (2016) The Architecture of the Cytoplasmic Region of Type III Secretion Systems. *Sci. Rep.* **6:** 33341

725 Mauracher CA, Gillam S, Shukin R & Tingle AJ (1991) pH-dependent solubility shift of rubella virus capsid
726 protein. *Virology* **181:** 773–777

727 McClements DJ & Li Y (2010) Review of in vitro digestion models for rapid screening of emulsion-based
728 systems. *Food Funct.* **1:** 32

729 Meuskens I, Saragliadis A, Leo JCC & Linke D (2019) Type V Secretion Systems: An Overview of Passenger
730 Domain Functions. *Front. Microbiol.* **10:** 1–19

731 Miesenböck G, De Angelis DA & Rothman JE (1998) Visualizing secretion and synaptic transmission with pH-
732 sensitive green fluorescent proteins. *Nature* **394:** 192–5

733 Milne-Davies B, Helbig C, Wimmi S, Cheng DWC, Paczia N & Diepold A (2019) Life After Secretion—Yersinia
734 enterocolitica Rapidly Toggles Effector Secretion and Can Resume Cell Division in Response to
735 Changing External Conditions. *Front. Microbiol.* **10:** 2128

736 Morimoto Y V, Kojima S, Namba K & Minamino T (2011) M153r mutation in a ph-sensitive green fluorescent
737 protein stabilizes its fusion proteins. *PLoS One* **6:** e19598

738 Mota LJ, Journet L, Sorg I, Agrain C & Cornelis GR (2005) Bacterial injectisomes: needle length does matter.
739 *Science (80-.).* **307:** 2005

740 Mühlenkamp M, Oberhettinger P, Leo JCC, Linke D & Schütz MSS (2015) Yersinia adhesin A (YadA) - Beauty

741 & beast. *Int. J. Med. Microbiol.* **305:** 252–258

742 Nakamura S, Kami-ike N, Yokota JP, Kudo S, Minamino T & Namba K (2009) Effect of Intracellular pH on the
743 Torque?Speed Relationship of Bacterial Proton-Driven Flagellar Motor. *J. Mol. Biol.* **386:** 332–338

744 Nans A, Kudryashev M, Saibil HR & Hayward RD (2015) Structure of a bacterial type III secretion system in
745 contact with a host membrane in situ. *Nat. Commun.* **6:** 10114

746 Petrovska I, Nüske E, Munder MC, Kulasegaran G, Malinovska L, Kroschwald S, Richter D, Fahmy K, Gibson
747 K, Verbavatz J-M & Alberti S (2014) Filament formation by metabolic enzymes is a specific adaptation
748 to an advanced state of cellular starvation. *Elife* **3:**

749 Rappl C, Deiwick J & Hensel M (2003) Acidic pH is required for the functional assembly of the type III
750 secretion system encoded by Salmonella pathogenicity island 2. *FEMS Microbiol. Lett.* **226:** 363–372

751 Rocha JM, Richardson CJ, Zhang M, Darch CM, Cai E, Diepold A & Gahlmann A (2018) Single-molecule
752 tracking in live Yersinia enterocolitica reveals distinct cytosolic complexes of injectisome subunits.
753 *Integr. Biol.* **10:** 502–515

754 Ross J & Plano G V (2011) A C-Terminal Region of Yersinia pestis YscD Binds the Outer Membrane Secretin
755 YscC. *J. Bacteriol.* **193:** 2276–2289

756 Saragliadis A & Linke D (2019) Assay development for the discovery of small-molecule inhibitors of YadA
757 adhesion to collagen. *Cell Surf.* **5:** 100025

758 Schindelin J, Arganda-Carreras I, Frise E, Kaynig V, Longair M, Pietzsch T, Preibisch S, Rueden C, Saalfeld S,
759 Schmid B, Tinevez J-Y, White DJ, Hartenstein V, Eliceiri K, Tomancak P & Cardona A (2012) Fiji: an open-
760 source platform for biological-image analysis. *Nat. Methods* **9:** 676–682

761 Slonczewski JL, Rosen BP, Alger JR & Macnab RM (1981) pH homeostasis in Escherichia coli: measurement
762 by 31P nuclear magnetic resonance of methylphosphonate and phosphate. *Proc. Natl. Acad. Sci. U. S.*
763 *A.* **78:** 6271–5

764 Sory M-P, Boland A, Lambermont I & Cornelis GR (1995) Identification of the YopE and YopH domains
765 required for secretion and internalization into the cytosol of macrophages, using the cyaA gene fusion
766 approach. *Proc. Natl. Acad. Sci. U. S. A.* **92:** 11998–12002

767 Stingl K & De Reuse H (2005) Staying alive overdosed: How does Helicobacter pylori control urease activity?
768 *Int. J. Med. Microbiol.* **295:** 307–315

769 Tachiyama S, Chang Y, Muthuramalingam M, Hu B, Barta ML, Picking WL, Liu J & Picking WD (2019) The
770 cytoplasmic domain of MxiG interacts with MxiK and directs assembly of the sorting platform in
771 the Shigella type III secretion system. *J. Biol. Chem.*: jbc.RA119.009125

772 Taylor DJ, Krishna NK, Canady MA, Schneemann A & Johnson JE (2002) Large-scale, pH-dependent,
773 quaternary structure changes in an RNA virus capsid are reversible in the absence of subunit
774 autoproteolysis. *J. Virol.* **76:** 9972–80

775 Tertti R, Skurnik M, Vartio T & Kuusela P (1992) Adhesion protein YadA of Yersinia species mediates binding
776 of bacteria to fibronectin. *Infect. Immun.* **60:** 3021–3024

777 Tokunaga M, Imamoto N & Sakata-Sogawa K (2008) Highly inclined thin illumination enables clear single-
778 molecule imaging in cells. *Nat. Methods* **5:** 159–61

779 Wagner S, Grin I, Malmsheimer S, Singh N, Torres-Vargas CE & Westerhausen S (2018) Bacterial type III
780 secretion systems: a complex device for the delivery of bacterial effector proteins into eukaryotic host
781 cells. *FEMS Microbiol. Lett.* **365:**

782 Wolter S, Löschberger A, Holm T, Aufmkolk S, Dabauvalle M-C, van de Linde S & Sauer M (2012)
783 rapidSTORM: accurate, fast open-source software for localization microscopy. *Nat. Methods* **9:** 1040–
784 1

785 Young GM, Amid D & Miller VL (1996) A bifunctional urease enhances survival of pathogenic Yersinia
786 enterocolitica and Morganella morganii at low pH. *J. Bacteriol.* **178:** 6487–95

Yu X-J, Grabe GJ, Liu M, Mota LJ & Holden DW (2018) SsaV Interacts with SsaL to Control the Translocon-to-Effector Switch in the Salmonella SPI-2 Type Three Secretion System. *MBio* **9:** e01149-18

Yu X-J, McGourty K, Liu M, Unsworth KE & Holden DW (2010) pH sensing by intracellular Salmonella induces effector translocation. *Science (80-.).* **328:** 1040–3